



μ PIV measurements of the phase-averaged velocity distribution within wavy films

Andreas Metzmacher¹ · Sebastian Burgmann¹ · Uwe Janoske¹

Received: 31 October 2022 / Revised: 21 February 2023 / Accepted: 24 February 2023 / Published online: 1 April 2023
© The Author(s) 2023

Abstract

Thin-film flows are frequently used in process engineering and are therefore of great interest in research. In most cases, waves occur which have a positive effect on the material and heat transport and significantly influence the dynamics of the film flow. A combination of μ -particle image velocimetry and confocal chromatic distance measurement is used to measure phase-averaged flow velocities in naturally developed film waves. A trigger signal is sent to the PIV system and a recording starts when a wave reaches the wave crest threshold. This makes it possible to trigger the μ PIV system depending on the film thickness. The focus of this work is on the triggering of the wave crest. The functionality and quality of the measurements depend on the correct positioning of the confocal chromatic sensor, with the light spot at the level of the camera section. Simultaneously, the minimum, average, and maximum film thickness, as well as the wave amplitude and wave frequency, are recorded. Film flow is investigated on a glass plate at various angles (5° , 10° , 15°) of inclination, Reynolds numbers (30–200), and measurement positions. The results are compared with the theoretical solutions according to Nusselt. In addition, the influence of the tilt angle and the measuring position is explained. The measuring position, in particular, has a non-negligible influence since the characteristics of the film flow are largely dependent on the streamwise measuring position. Compared to the theoretical solutions according to Nusselt, the velocities and film thicknesses are significantly greater due to the presence of the waves. With increasing inclination angle and streamwise measuring position, the measured mean and maximum velocities of the film flow increase. They almost double when the inclination angle increases from 5° to 15° . When comparing the velocities depending on the measuring position (300–500 mm), it is noticeable that the velocities increase between 5 and 15%, depending on the angle, due to wave development and gravity.

List of symbols

a	Wave amplitude [m]
B	Channel width [m]
DOC	Depth of correlation [m]
f_w	Wave frequency [Hz]
F	Adjustment factor
Ka	Kapitza number
Re	Reynolds number
UL	Upper limit [m]
\dot{V}	Volume flow [l/h]
$w(z)$	Flow velocity [m/s]
w_{Nu}	Average flow velocity [m/s]
x	Measuring position [m]
x^*	Distance to the beginning of the wave [m]
y, z	Spatial coordinates [m]

Greek symbols

δ	Fluid thickness [m]
η	Dynamic viscosity [mPas]
λ	Wavelength [m]
ν_f	Kinematic viscosity [m ² /s]
ρ	Density [kg/m ³]
σ	Surface tension [N/m]
φ	Inclination angle of the plate [°]

1 Introduction

Liquid films are found in many technical applications, like falling film evaporators and packing columns (Helbig 2007). The film thickness δ and thus the characteristic velocity distribution within the film significantly determine the heat and mass transfer in many process engineering tasks. As a result of the hydrodynamic instability of the film flow and depending on the surface tension of the fluid, waves form on the fluid surface. Small high-frequency waves occur in the inlet region, which converge and collide downstream (Adomeit

✉ Andreas Metzmacher
metzmacher@uni-wuppertal.de

¹ Chair of Fluid Mechanics, Bergische Universität Wuppertal, Wuppertal, Germany

and Renz 2000; Ausner 2006; Brauner and Maron 1982; Kohrt 2012). As a result, the characteristic parameters, such as the wave frequency f_w and the average film thickness δ_{avg} , decrease on the way downstream until a state of equilibrium is reached (Takahama and Kato 1980). Thus, the wave formation and the resulting dynamics of the liquid film exhibit a pronounced dependence on the run length. In addition, the formation of waves and the attainment of the equilibrium state are significantly influenced by the inclination angle of the wetted surface, the flow rate and the material properties.

In the inlet area, the flow velocity, as well as the film thickness, agree very well with the theoretical solution according to Nusselt (Nusselt 1916; Takamasa and Kobayashi 2000). Unfortunately, the effect of run-length and inclination on the formation of the characteristic velocity distribution within the film is still unclear. It is known that with increasing distance to the inlet, the deviation from the theoretical solutions increases. Additionally, it is known that at high inclination angles and low flow rates, the steady-state wave characteristics are reached after a shorter run length (Brauner and Maron 1982; Brauner and Maron 1983).

Measurements of the surface velocity of thin vertically falling liquid films have been performed by Ishigai et al. (1972). Thin aluminum plates (0.04 mm^2) floated on top of the film flow. The surface velocity was investigated via the distance traveled between the photos. It was shown that the surface velocities of wavy films are about twice as large as those according to Nusselt.

Alekseenko (1985) used the integral relations method to derive a nonlinear two-wave equation for long waves on the surface of vertically falling excited liquid films on tube walls. The method was confirmed with experimental measurements of instantaneous velocity profiles at Reynolds numbers of 5–50. For this purpose, a combination of the shadow method to measure film thickness and the stroboscopic particle method to measure velocities was used.

Mudawar and Houpt (1993) investigated the role of large waves in the transport of mass and momentum in vertically falling fluid films on a pipe outer wall. They simultaneously investigated the time-varying film thickness with a film thickness probe and the flow velocity with laser doppler velocimetry (LDV) at a measuring position of 1842.5 mm for Reynolds numbers from 209 to 414. It has been shown that about 40–70% of the flow is transported by large waves and that they behave like clumps of fluid sliding over a continuous substrate, while the substrate remains relatively unaffected.

Miyara (1999) numerically investigated the fluid dynamics and heat transfer of falling fluid films on a vertical plate. The velocity profiles of the different positions in the wave were compared with those of a laminar flow. The velocities at the wave crest and in the wave trough are very different from a laminar film flow, while the profiles at the wave rear

and in the substrate region are very similar to a laminar flow. It was also determined that the time-averaged velocity profile in the region of the minimum film thickness, corresponds to that of the Nusselt theory.

Adomeit und Renz (2000) investigated laminar wavy film flows in the Reynolds number range from 27 to 200. Measurements of the velocity distribution are made by particle image velocimetry and film thickness measurements by fluorescence methods. The measurement plane is perpendicular to the tube wall and parallel to the tube axis. ZrSiO_4 particles with an average diameter of $1.8 \mu\text{m}$ are used as tracer particles. The data of the velocity measurements differ greatly from those according to Nusselt. In the apex of the large waves, the flow velocities, with the same Nusselt film thickness δ_{Nu} , show values about 25–40% lower than the Nusselt solution. However, as in Ishigai et al. (1972) the surface velocity is more than twice that of the Nusselt solution. Waves already occur at small Reynolds numbers. As a result, the film flow can be divided into a layer close to the wall, the so-called base film, and the wave layer close to the surface. Investigations by Adomeit und Renz (2000) and Miyara (1999) could show that the Nusselt profile of the velocity distribution is only valid for the base film and deviates strongly from it in the wave layer. Therefore, this type of flow is called *pseudolaminar*.

Al-Sibai (2004) investigated characteristic parameters such as wave velocity and fluid flow velocities on an inclined flat Plexiglas plate. The wave velocity was determined using a cross-correlation of two film thickness measurements. From the determined time of the cross-correlation and the constant distance between the gauges ($\Delta x = 2.9 \text{ mm}$), the wave velocities can be calculated. It was found that due to the different wave heights, the wave speed has a range dependent on the Reynolds number. In addition, particle image velocimetry measurements were made perpendicular to the film, through the sidewall, at Reynolds numbers from 1.4 to 60. A highly viscous fluid was chosen to avoid waves, since the flow velocity within the waves cannot be measured sufficiently well by the measurement technique. The flow velocities in the film, which is as free of waves as possible, agree very well with the theoretical Nusselt profile.

In his work, LeI et al. (2005) presented two different methods for measuring the thickness of wavy films. The first is a new non-intrusive technique called chromatic confocal imaging method. The accuracy of this technique depends on the optical components, the local gradient of the film thickness, and the accuracy of the refractive index used. LeI et al. (2004) showed that showed that the average film thickness data thus obtained agreed well with earlier experimental measurements. The second technique for simultaneous measurement of film thickness and wave speed is based on a fluorescence intensity technique. Here, film thickness and wave speed measurements of silicone films with different

viscosities were studied for Reynolds numbers from 2 to 700 and different tilt angles. The experimental data are in good agreement with results from published experimental and theoretical studies. The minimum measurable film thickness with the confocal chromatic sensor in this work was in the range of 200 microns. It was shown that for most film flows the amplitude of the waves is small compared to the wavelength and the measurement error due to film curvature is only about 3 μm .

Ausner (2006) investigated the surface velocity of liquid films on a 60° inclined flat plate to identify influences of the feed type. An overflow weir and a feed pipe with multiple holes have been investigated as feed types. The water and water-toluol flow are inoculated with ceramic isospheres SG-300B, which float on the surface of the film flow. In order to identify the surface velocities, the images of the particle images (50 particles or waves) are manually evaluated and compared. It could be shown that the velocities, when fed with the feeder tube, are greater than the Nusselt solution, while those of the overflow weir are lower. For example, the surface velocity according to Nusselt for $\text{Re} = 190$ is exactly between those of the two feed types.

Dietze et al. (2009) were able to show numerically and experimentally that for excited waves at Reynolds numbers of 8.6–15, flow separation occurs in the capillary wave region of falling liquid films within a tube. For this purpose, the methods of LDV and particle image velocimetry (PIV) were used to detect velocities in the capillary wave range. A confocal chromatic sensor was used to make simultaneous layer thickness measurements to correlate the velocity data with the wave dynamics. Using PIV, the existence of a separation vortex in the capillary wave region was shown. Due to the time-varying refraction effects of waves, a PIV measurement through the fluctuating phase interface is associated with measurement inaccuracies. Paschke (2011) developed an adapted μPIV measurement technique with a correction unit to reduce these inaccuracies in order to measure directly through the gas-liquid phase interface. As part of the work, Paschke validates this with the conventional μPIV technique through a transparent wall. For this purpose, measurements are performed with water-glycerol mixtures, on an inclined (45° and 60°) flat plate, at Reynolds numbers of 2–256. For the μPIV images, fluorescent particles were used, which are excited with the laser. In combination with a cut-off filter, only the fluorescence wavelength ($\lambda_{\text{particle}} > \lambda_{\text{Laser}}$) passes the filter. This has the advantage that the particles are clearly displayed without background illumination. The measurements show good agreement between the new and the conventional measurement methodology as well as the theoretical solution according to Nusselt. After successful validation, measurements were performed on structured plates, as well as tetrahedral structures.

In their work, Charogiannis et al. (2015) investigate the hydrodynamic parameters of harmonically excited film flows on a flat soda-lime glass plate, which was tilted by 20°. A simultaneous measurement technique based on planar laser-induced fluorescence imaging (PLIF) and particle image/tracking velocimetry (PIV/PTV) is used for the investigation. A total of four water-glycerol mixtures with different Kapitza numbers Ka , as well as a Reynolds number range from 2.3 to 320 are investigated. Frequencies from 1 to 10 Hz are imposed on the film flow. Based on these data, velocity profiles of 20 sites along the wave topology are extracted and compared with analytically derived ones based on local film thickness measurements and the Nusselt solution. It is found that increasing the ripple by modulating the drive frequency leads to lower absolute deviations between experiments and theoretical predictions upstream of the crests and higher deviations downstream of the crests. At the crests, experimentally determined interfacial velocities are overestimated by almost 100%.

For high-resolution velocity measurement of thin liquid film flows on an inclined smooth glass plate, a combination of confocal chromatic distance measurement and μPIV is presented in this work. This combination makes it possible to obtain velocity data directly for defined positions in the flow, instead of having to match them using temporal film thickness data. The focus is on the determination of velocities in the wave crest, of naturally evolving film flows. The flow is not captured laterally, as is usually the case, but is scanned stepwise from below through the transparent plate across the film thickness and extended by wave triggering. This means that the flow profiles are not acquired instantaneously but averaged over several selected waves.

2 Experimental setup

The film flow passes through a 1500 mm long and 300 mm wide glass channel. Hence, boundary effects can be minimized. The channel can be oriented at any angle φ . The fluid is pumped by a centrifugal pump to the overflow weir. Depending on the impeller sensor, the volume flow can be adjusted via a mass flow controller in the ranges 0–100 l/h and 60–1800 l/h. Excess volume flow is returned to the collector-tank via a bypass valve. To compensate the pump-heat, a water-cooling system is integrated downstream of the mass flow controller. This consists of several Peltier elements and two temperature sensors in the overflow weir, which keep the fluid at a constant temperature of 22 ± 0.2 °C via an aluminum heat sink. The fluid slowly rises in the overflow weir until it flows purely gravitationally, initially as a smooth film along the channel, and is collected again in the collection tank, creating a closed circuit. To record the particles, the PIV camera (ILA.PIV.Nano) is located below

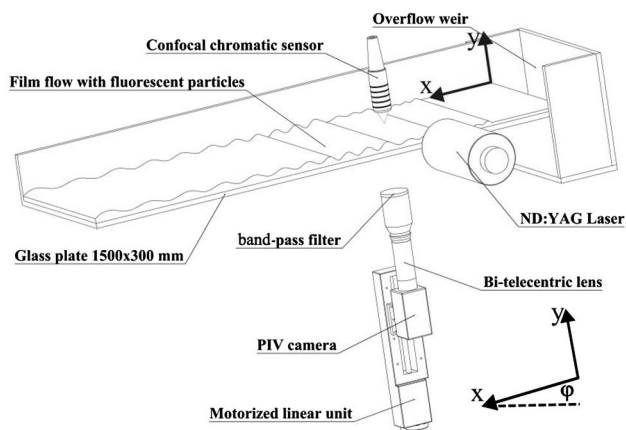


Fig. 1 Schematic representation of the experimental setup for the investigation of thin film flows on inclined smooth planes. The fluid flows from the overflow weir into the glass channel purely gravitationally driven and forms waves which develop on the way downstream

the glass channel to avoid time-varying refraction effects at the gas-liquid phase interface. The camera has a 2/3" sensor with a resolution of 1392×1040 pixels with a pixel size of $6.45 \times 6.45 \mu\text{m}$. A bi-telecentric lens (SILL TZM 2533/3.0) with a magnification of 3 is used. This results in a maximum object size of $2.9 \text{ mm} \times 2.2 \text{ mm}$. The scaling factor required for PIV evaluation is 467 px/mm and was determined using a microscope-object-micrometer, with a scale of $1/100 \text{ mm}$. The camera and thus the position of the focal plane is moved by the motorized linear unit LTM 60–150-HSM from OWIS, which travels plane by plane. A 10 Hz ND:YAG double-pulse laser (Evergreen from Quantel) with a wavelength of $\lambda_{\text{Laser}} = 532 \text{ nm}$ is used. The laser light is formed into a thin slice of light with a cylindrical lens but still illuminates the complete film. The film flow is seeded with fluorescent polystyrene particles with an average diameter of $4.99 \mu\text{m}$ at a density of 1050 kg/m^3 . Excitation of the laser light causes the particles to emit fluorescent radiation ($\lambda_{\text{Particle}} = 607 \text{ nm}$), which, unlike laser light, can pass the bandpass filter ($575 \text{ nm} \times 50 \text{ nm}$, optical density 4.0 50 nm from Edmund optics) because of the Stokes shift. The confocal chromatic sensor IFS2405-3, from micro-epsilon, is positioned above the channel, directly above the camera, and records the film thickness over time $\delta(t)$. In combination with the controller IFC2421, measuring rates of up to 6.5 kHz are possible with the sensor. Due to the reduced measuring range at 6.5 kHz, a measuring rate of 1.5–4 kHz is used depending on the film thickness. The measuring range is three millimeters with a resolution of 15 nm (Fig. 1).

The following parameters have been varied: the inclination angle ϕ (horizontal, 5° , 10° , 15°), the measuring position (150, 300 and 500 mm), as well as the Reynolds number Re (30–200) at variation of the volume flow rate (\dot{V}). The fluid

Table 1 Material properties of demineralized water at 22 °C. The density and dynamic viscosity are taken from the VDI-Wärmeatlas (2013)

Fluid	ρ [kg/m^3]	η [$\text{mPa} \cdot \text{s}$]	σ [mN/m]
Demineralized water	997.77	0.954	72.14

The surface tension was determined by the ring method according to Du Noüy

used is demineralized water with the following properties. The fluid used is demineralized water (Table 1).

3 μ Particle image velocimetry

μ Particle Image Velocimetry is used to measure the flow profiles of naturally wavy film flows. The focal plane is not defined by the laser light section, but by the position of the depth of field. To achieve the smallest possible depth of field, the aperture is set to F1.6 at maximum. This results in a depth of field of approx. $18.87 \mu\text{m}$. The depth of correlation DOC was estimated using the equation of Olsen and Adrian (2000) and is $57 \mu\text{m}$. Note, due to image pre-processing that eliminates blurry low-gray-value patterns, the depth of correlation is in fact slightly smaller. The refractive index of the fluid is accounted for when shifting the planes. A camera step size of $30\text{--}50 \mu\text{m}$ is chosen to scan the complete film resulting in up to 20 measurement planes (in case of a wave, i.e., Fig. 4). Smaller step sizes up to $1 \mu\text{m}$ are possible, but not necessary because of the depth of correlation. 450 double-exposed images respectively waves are captured per measuring plane. The camera is then shifted so that the next film plane is recorded.

Due to the shallow depth of field, very few particles are present in the images. As in the work by Paschke (2011), an image addition of the double images is performed to increase the particle density in the images. Figure 2 shows the ratio of white to black pixels as well as the number of particles per pixel as a function of the film plane of an approximately 1 mm high film flow.

Here, the particles are normally distributed within the film flow. Most of the particles are located in the middle part of the film flow, while the number of particles decreases significantly in the lower and upper part. By adding the particle images, the particles in the images increase significantly, but they are still normally distributed. In order to obtain the same number of particles in each layer as possible, a variable addition is performed. Depending on the layer, different numbers of images (for A and B each) are added, since there are enough particles in middle film layers and an overlapping of these should be avoided. To determine the addition number, the ratio of white to black pixels of the added images of each layer is determined. If this value is

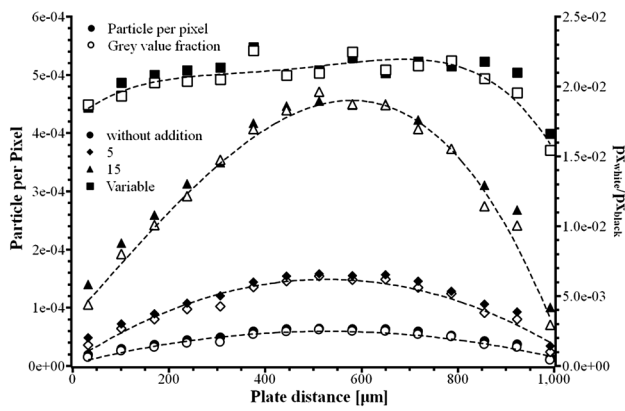


Fig. 2 Example of particles per pixel and the ratio of white to black pixels as a function of film thickness. Illustration of the influence of image addition to increase the particle density. The symbols show the corresponding curves with no addition ●, a fixed addition number of 5 ◆ and 15 ▲ images, and variable addition ■ for each layer

still too low, additional images are added until the specified ratio or a maximum number of added images is reached. The threshold was chosen to ensure that a sufficient number of particles occur in each interrogation window. The small number of particles can be significantly increased in Fig. 3 by adding 5–40 images allowing smaller interrogation windows to be selected.

After the addition of the images for each plane, the evaluation of them is performed. For data analysis and image processing the software PIVview2C and PIVscheduler from ILA_5150 GmbH is used. The size of the interrogation area is 128×128 , 256×256 or 512×512 pixels with an overlap of 50% depending on the final particle density. In addition, blurred particles that do not originate from the focal plane are eliminated in the PIV software by using a median filter. Due to the flow, without, e.g., the occurrence of vortices and in combination of the large interrogation windows, no spurious vectors occur.

Figure 4 represents the vector fields for each plane in the left figure. An averaged velocity for each plane is calculated from the individual vectors in the left figure and this is plotted over the film thickness as shown in the right figure. Here, the error bars of the axis of the flow velocity represent the standard deviation σ of all velocities of a plane and the axis of the plate distance represents the deviation of the focal plane due to the depth of field. According to the wall adhesion, the velocity should be 0 mm/s for $y=0$. When compared with the approximated velocity profile, it is noticeable that for $y=0$ the velocity is greater than 0 mm/s. This is due to the fact that fewer particles are present in lower film levels. As can be seen in Fig. 2, fewer particles are located at lower and higher levels of the film flow. Due to the depth of field, more particles are detected in higher film planes, which have higher velocities and thus the average velocity

is slightly increased. In addition, reflections of particles may occur when measuring near the glass surface. These reflections also have higher velocities than particles near the wall would have.

Wave triggering is intended to allow the detection of the flow profile at any points in the wave. Here the focus is on the wave crest. The maximum and minimum limit values can be defined in the software of the confocal chromatic sensor, which also makes it possible to examine the wave front or the back of the wave. Simultaneously to the μ PIV images, the local film thickness $\delta(t)$ is recorded (1.5–4 kHz) using a confocal chromatic sensor. The choice of the measuring rate results from the Reynolds number and the wave amplitude. The factor F is used because not every wave reaches the maximum film thickness and varies between 0.1–0.125 depending on the parameter combination. When an upper limit value UL (wave crest) is reached:

$$UL = \delta_{\max} - F \cdot a \tag{1}$$

a 5 V TTL signal is generated by the control unit of the confocal chromatic sensor and sent to the synchronizer of the PIV system. UL is calculated using the maximum film thickness δ_{\max} as well as the wave amplitude a ($\delta_{\max} - \delta_{\min}$). The values are determined directly before the PIV measurements, by three measurements per 60 s with the confocal chromatic sensor. In addition, the average film thickness δ_{avg} and the wave frequency f_w are also calculated from the measured film thickness over time. The difficulty of triggering is to have the wave specifically in the image section, otherwise no particles can be detected at higher film thicknesses. This can be counteracted by setting the focus level to the height of the wave crest at the beginning of the PIV measurements and checking whether particles are in the camera window or not.

4 Results

The decisive influencing factors in the investigations were the angle of inclination of the channel, as well as the Reynolds number, which can be determined according to equation:

$$Re = \frac{\dot{V}}{v_f \cdot B} \tag{2}$$

This was set at constant kinematic viscosity ν_f and channel width B by varying the volume flow. Figure 5 exemplarily shows the phase-averaged velocity profile just within the wave for case $\varphi = 10^\circ$ and $Re = 50$. I.e. this velocity distribution was measured in the wave region. The velocity profile still exhibits a similar shape as the theoretical Nusselt profile. In this case, the Nusselt profile is also plotted to

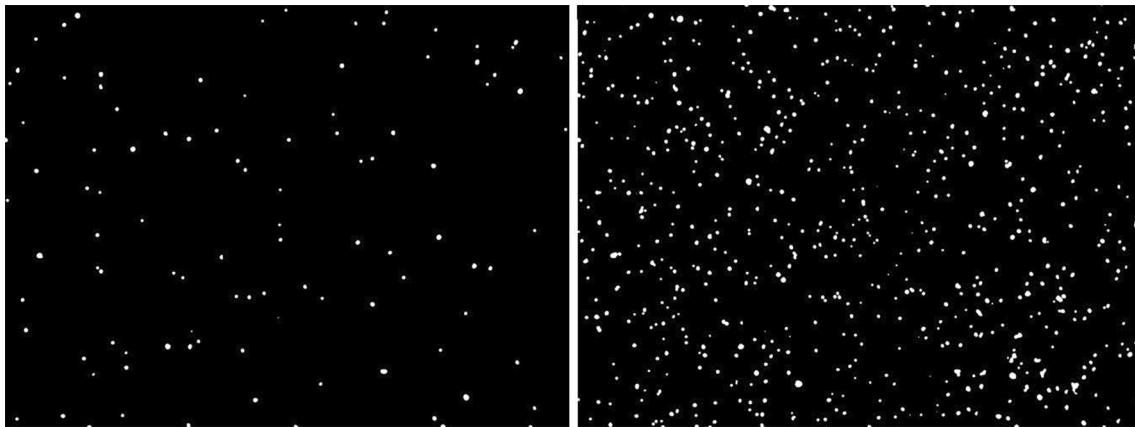


Fig. 3 Single particle image (left) with low particle image density and a particle image (right) with increased particle image density after image addition. Addition ensures a more even distribution of particles and ensures that there are always particles in the interrogation windows

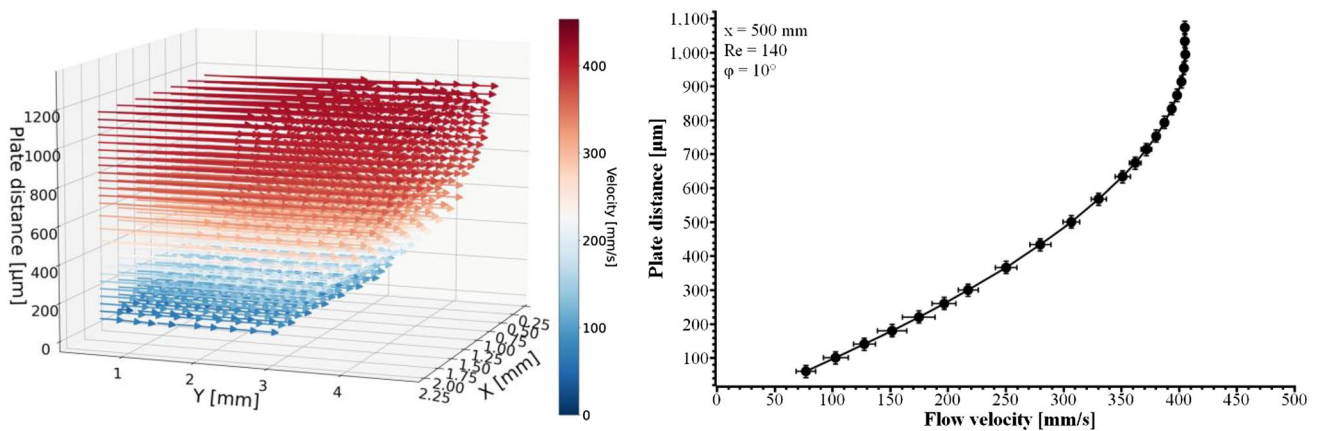


Fig. 4 Vector fields for each plane of the film flow with 128×128 query windows (left) and calculated flow profile from the mean values of the individual vector fields (right) for $Re = 140$ at $x = 500$ mm and a tilt angle of 10°

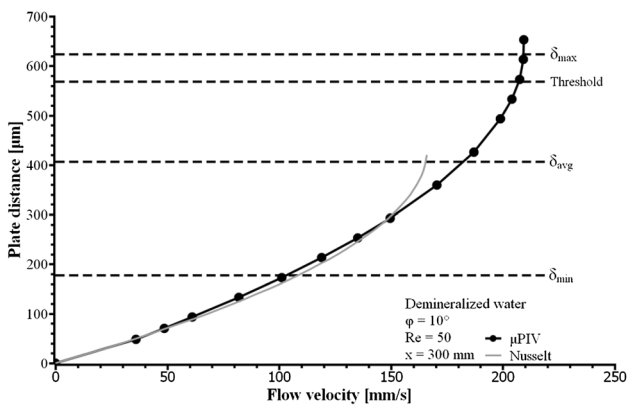


Fig. 5 Example of a velocity profile with wave triggering compared to the Nusselt velocity profile for $Re = 50$ at an angle of inclination of 10° and $x = 300$ mm

illustrate the theoretical velocity distribution in the temporal average.

Note, the Nusselt equations only apply exactly to waveless liquid films. However, it is widely used for the wavy part as well. As can be seen in Fig. 5 the waves lead to a fast transport of fluid in the upper part of the film (about 1.25 times faster than the maximum velocity in the mean case). However, in the lower part the velocity profiles are almost identical. This is a hint that the film can be divided into a base film part ($< \delta_{min}$) and a wave-part. In the base film, the flow can be assumed to be almost laminar. Furthermore, the theoretical and measured velocities in the base film are almost identical and differ strongly from each other in the wave range, which again confirms the results of Adomeit and Renz (2000) as well as Miyara (1999). Shortly before reaching the minimum film thickness (start of the wave part), the velocity profiles start to deviate from each other. This may be the influence of the

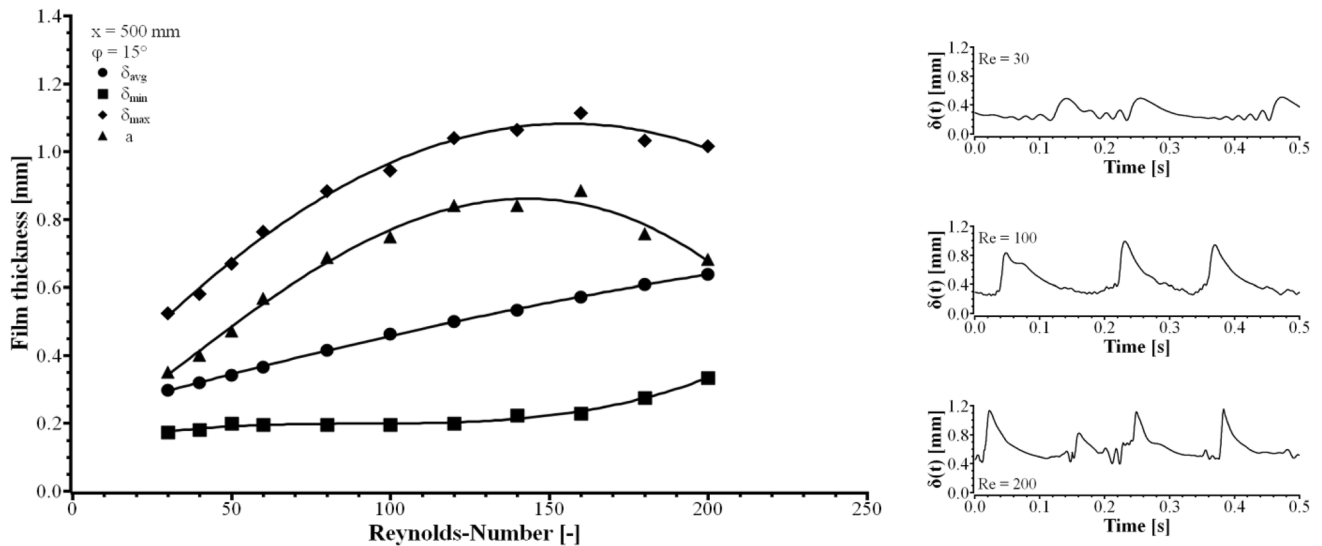


Fig. 6 Minimum, average and maximum film thicknesses and wave amplitudes as a function of Reynolds number (left) at a measuring position of 500 mm and an inclination angle of 15°. Additionally,

a selection of temporal film thickness profiles (right) for Reynolds numbers 30, 100 and 200 in descending order

wave layer sliding on the base film. To illustrate the size of the waves, the film thicknesses and wave amplitude for different Reynolds numbers, for a measurement position at 500 mm and an angle of 15° are shown in Fig. 6. On the right, three selected film thickness curves are shown for a better estimation of the existing local wave characteristics.

Here it is noticeable that the minimum film thickness δ_{\min} is almost constant at about 0.2 mm. Accurate positioning of the confocal chromatic sensor is essential, otherwise a trigger signal may be released even though there is no wave directly above the camera. This leads to incorrect measurements. The minimum wave amplitude over all tests, occurs at a low inclination angle of 5° and a short distance to the inlet ($x=150$ mm) and is 0.01 mm. No wave triggering is necessary here, since the film is smooth. On the other hand, at 15° and a Reynolds number of 160, the largest wave amplitude of about 0.88 mm occurs at the measuring position of 500 mm. Depending on the angle, measuring position and Reynolds number, wave triggering may or may not be necessary. Contrary to expectations, larger Reynolds numbers have a longer waveless range, which means that wave triggering is not always necessary for small measuring positions ($x=150$ – 300 mm) and large Re. The distance x^* to the beginning of the wave formation can be estimated as follows:

$$x^* \approx 500 \cdot \delta_{\text{avg}}, \text{ for } Re < 500 \tag{3}$$

according to Brauner and Maron (1982). Due to the fact that the wave formation starts later with larger Reynolds numbers, smaller Re can have a larger maximum film thickness at the same measuring position, since this is significantly

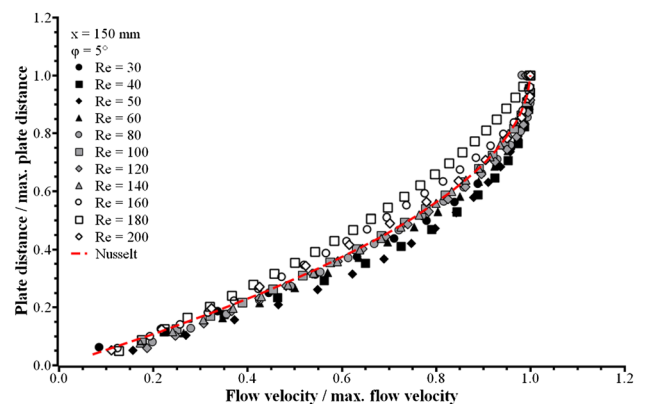


Fig. 7 Dimensionless representation of the μ PIV flow profiles at 150 mm and $\varphi=5^\circ$ compared to the dimensionless solution according to Nusselt

influenced by the waves. This results in a decrease of the wave amplitude in Fig. 6 from Re = 160. Figure 7 shows the dimensionless flow profiles at a distance of 150 mm from the inlet and an inclination angle of 5° for all investigated Reynolds numbers. In addition, the theoretical Nusselt velocity profile is also shown normalized as a red dashed line. This is calculated as follows:

$$w(z) = \frac{g \cdot \sin\varphi \cdot \rho \cdot \delta_{\text{Nu}}^2}{2 \cdot \eta} \cdot \left[\frac{2 \cdot z}{\delta_{\text{Nu}}} - \left(\frac{z}{\delta_{\text{Nu}}} \right)^2 \right] \tag{4}$$

This is largely determined by the inclination angle φ , the density ρ of the fluid, the theoretical Nusselt film thickness

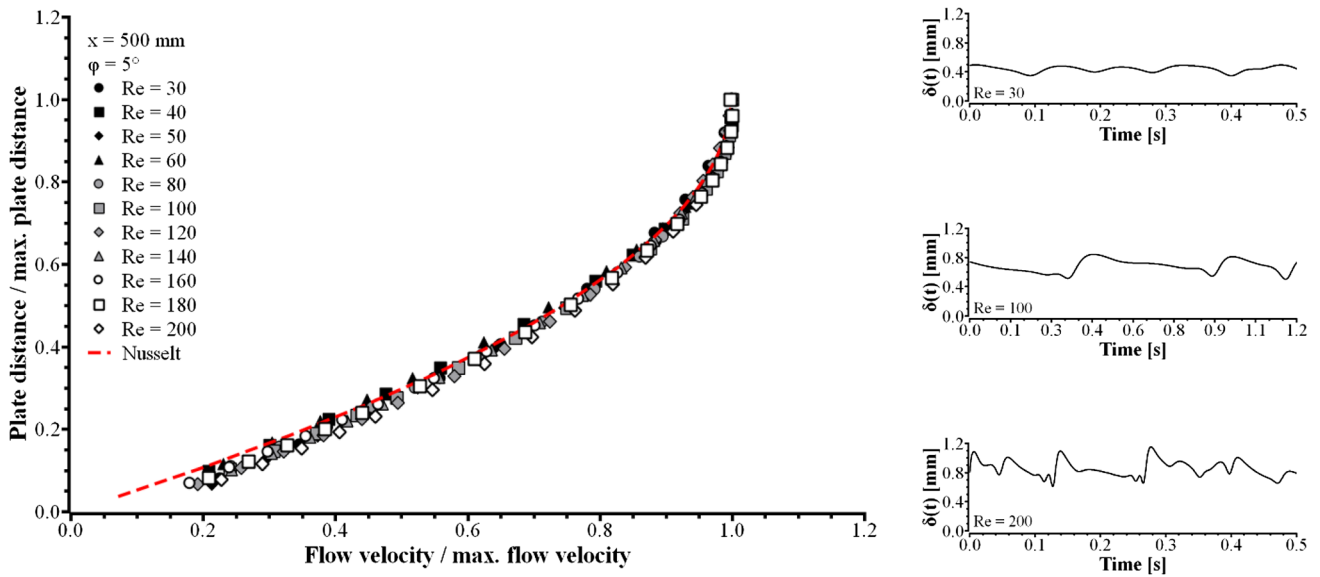


Fig. 8 Dimensionless representation of the μ PIV flow profiles at 500 mm and $\varphi = 5^\circ$ compared to the dimensionless solution according to Nusselt. Additionally, a selection of temporal film thickness profiles (right) for Reynolds numbers 30, 100 and 200 in descending order

δ_{Nu} , and the dynamic viscosity η . The average flow velocity w_{Nu} can be calculated as follows:

$$w_{Nu} = \sqrt[3]{\frac{g \cdot \sin\varphi \cdot v_f}{3}} \cdot Re^{\frac{2}{3}} \tag{5}$$

The Nusselt film thickness δ_{Nu} also depends on the angle φ , the kinematic viscosity v_f and the Reynolds number Re :

$$\delta_{Nu} = \sqrt[3]{\frac{3 \cdot v_f^2}{g \cdot \sin\varphi}} \cdot Re \tag{6}$$

Due to the inclination angle of $\varphi = 5^\circ$, at this measuring position $x < x^*$ is for all cases. This leads to a larger scatter around the dimensionless Nusselt profile. In addition, it is possible that inlet effects at the overflow weir, at measuring positions close to the inlet, be also an issue for the strong scattering of the data. Interestingly, for smaller Reynolds numbers the velocity profiles exhibits a bulgier shape, whereas higher Reynolds numbers show a straighter curve above the theoretical solution. For larger angles (10° , 15°), at the measurement position of 300 mm $x > x^*$ for most cases. Compared to Fig. 7, the measured data are closer to the theoretical solution according to Nusselt.

At a measuring position of $x = 500$ mm, the film flow has already developed more strongly. Due to the effect of gravitation and wave formation, higher flow velocities occur compared to the measuring position of $x = 150$ mm. The scatter of the data is also significantly lower as can be seen in Fig. 8. Compared to the tilt angles 10° and 15° , the scatter

of the data is also smaller. This could be due to larger wave amplitudes and a wider wave spectrum at angles $10\text{--}15^\circ$.

4.1 Influence of the angle of inclination

Figure 9 shows three velocity profiles at different angles. The Reynolds number and measuring position are identical. According to equations Eqs. (4) and (6), the velocity of the film flow increases with increasing inclination angle, but the film thickness decreases according to Nusselt. However, these equations do not consider the occurrence of waves.

Despite the different angles, the maximum film thicknesses of the individual profiles are almost the same. Although the average film thicknesses are smaller with increasing angles, the maximum film thickness is defined by the appearance of waves on the film. The flow velocity increases with increasing angles as expected. Measuring position 300 mm: When the tilt angle increases from 5° to 10° , the average velocity increases by about 45% and the maximum velocity by about 43%, averaged over $Re = 30\text{--}200$. Here, the differences are larger for the small Reynolds numbers ($\approx 60\%$) than for the larger Re ($\approx 33\%$). This is due to less developed waves at larger Reynolds numbers and low measurement positions. When the tilt angle increases from 5° to 15° , the average speed increases by about 87% and the maximum speed by about 77%. Here, the differences in the mean velocity at $Re = 30\text{--}80$ ($\approx 110\%$), are about twice as large as at $Re = 160\text{--}200$. The same applies to the maximum velocity. At a distance of 500 mm from the inlet, the velocity differences for the larger Reynolds numbers approach ($< 15\%$) those of the smaller ones. This

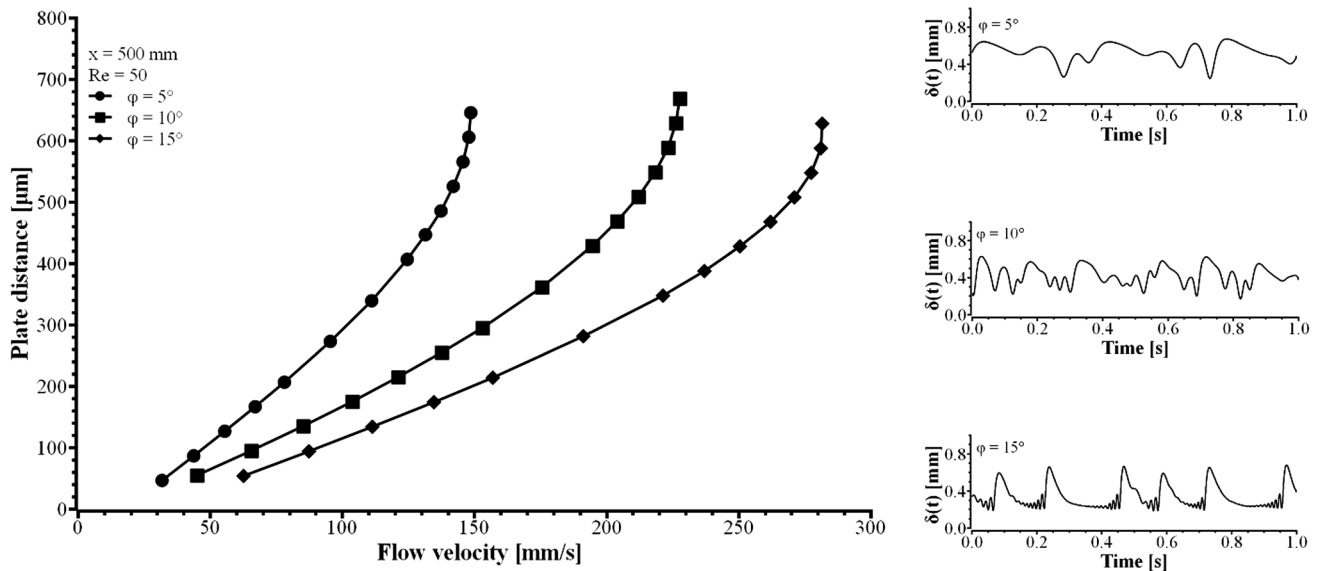


Fig. 9 Comparison of the velocity profiles (left) at different tilt angles for $Re=50$ at the measuring position $x=500$ mm. In addition, the corresponding time profiles (right) of the film thickness for 5° , 10° and 15°

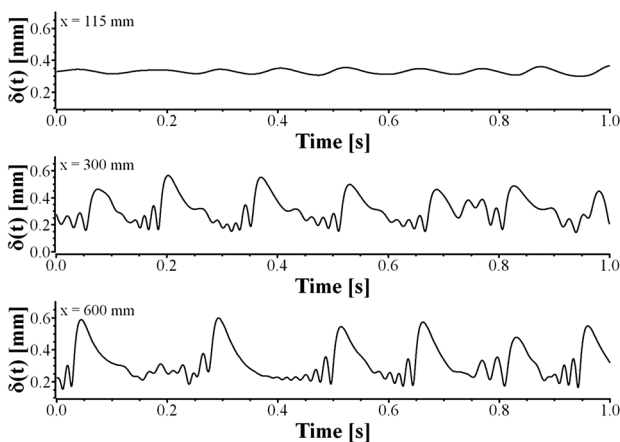


Fig. 10 Extract of the local film thickness measurements with the confocal sensor at the measuring positions 115 mm, 300 mm and 600 mm to show the wave development as a function of the distance to the inlet for $Re=40$ and $\varphi=15^\circ$

increase is due to the fact that the waves have a greater distance to travel before reaching the measuring position and can develop more.

4.2 Influence of the measuring position

Due to the wave development, the measurement position has a strong influence on, for example, the wave frequency and flow velocity. As an example, Fig. 10 shows the film thickness curves over time at three measuring positions.

At first, small sinusoidal surface waves are formed at the inlet, which collide and increase with increasing distance.

The waves increase in size, i.e., the wave amplitude increases. In addition, the wave frequency decreases over the run length. It can be seen that more distinct wave crests form, which are followed by many smaller waves ($x=300$ mm). At greater distances from the inlet ($x=600$ mm), the wave crests are even more distinct and a short plateau forms between the waves, the so-called residual film. This occurs more or less developed, depending on the inclination, Reynolds number and measuring position.

Figure 11 shows the flow velocities of the individual Reynolds numbers at an inclination angle of 15° . It is noticeable that the flow velocities as well as the maximum film thickness increase with a further distance to the inlet. When comparing the measurement positions ($x=300$ – 500 mm), the average flow velocity increases between 5 and 13%, depending on the angle. For the maximum flow velocity, the differences are between 6 and 16%, due to the gravitational influence of the inclined plate and the more developed waves that move faster on the base layer. The difference is particularly large at the higher Reynolds numbers. This is due to the fact that these have a significantly longer wave-free range, so that no or very small waves occur at $x=300$ mm. The maximum film thickness at $Re=140$ – 200 increases by $\approx 50\%$ on average due to the waves. The wave amplitude even $\approx 250\%$.

4.3 Comparison with the theoretical solution according to Nusselt

In Fig. 12 (left), the mean velocities are compared with those according to Nusselt, for the same Reynolds number. Almost all data show significantly higher velocities. The deviation

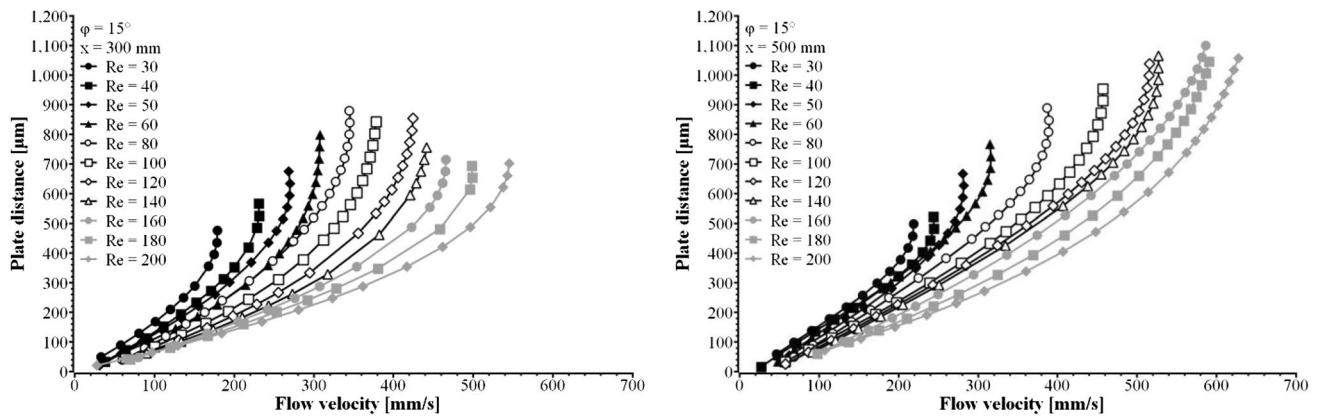


Fig. 11 Comparison of velocity profiles of film flows in for Reynolds numbers $Re = 30\text{--}200$ and measurement positions

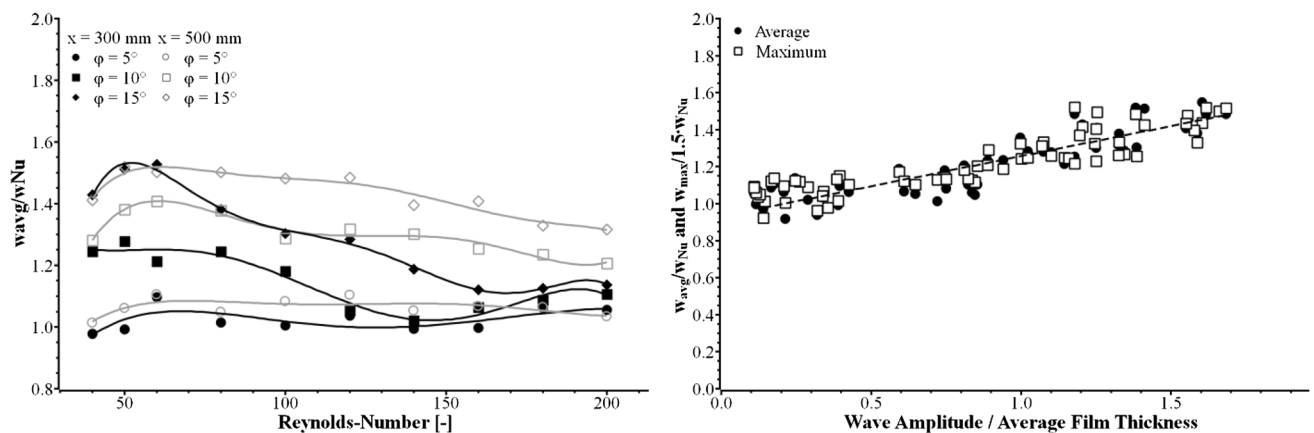


Fig. 12 Ratio of the obtained average velocities of the flow profiles to the theoretical solutions according to Nusselt as a function of the measuring position as well as the Reynolds number (left). Ratio of the mean and maximum measured velocities of the flow

from Nusselt also increases with increasing angle. This is due to the occurrence of large waves, which are not considered according to the theoretical solution. Only smaller angles (5°) agree well with the solution according to Nusselt, since fewer or very small waves occur. The deviations of the maximum velocity to Nusselt, are comparable to those of the mean velocity.

The right figure shows the influence of the waviness on the deviation from the theoretical values according to Nusselt in more detail. On the x-axis, a ratio of wave amplitude to measured average film thickness is formed in order to obtain an influence of the waviness. The y-axis shows the ratios of the mean and maximum flow velocities with the corresponding theoretical velocities. Here, $w_{\text{avg}}/w_{\text{Nu}} = 1$ means that the data are identical to the theory and $w_{\text{avg}}/w_{\text{Nu}} > 1$ means that the measured flow velocities are greater. The data show that with a larger fraction of wave amplitude, i.e., larger waviness, the deviation increases, and at a low waviness, the data agrees well with the theory. It can

also be seen that the deviations of the average and maximum flow velocities are almost identical.

4.4 Comparison with and without wave triggering

The potential of the wave triggering is shown in Fig. 13. Common PIV measurements without triggering have the disadvantage that images without particles are taken when waves occur. This has a negative effect on the quality of the results. An alternative is to take a plurality of images and do not use the empty images. This procedure represents the gray curve.

In the wave-free region, the flow velocities are almost identical. Shortly before reaching the minimum film thickness, start of the wave layer, the two curves begin to diverge. Here, apparently, a first influence of the wave layer becomes noticeable. Without wave triggering, all kind of waves, that do not reach the maximum film thickness are also considered, which can lead to velocity gradients within the added particle images and to lower determined flow velocities. As

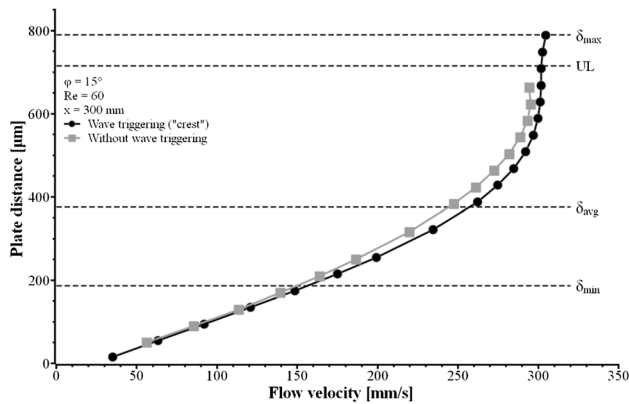


Fig. 13 Representation of the flow profiles, for $Re=60$ at a tilt angle of 15° and $x=300$ mm, with and without using the wave triggering. Image addition was used for both cases

can be seen here, different velocity profiles in the wavy area are calculated from the particle images. Furthermore, a few less layers could be detected than with triggering, since most of the images were without particles. This could possibly be compensated with a larger number of images.

5 Conclusion

In the paper, a combination for detecting the velocities of naturally evolving film flows at small tilt angles on a flat plate with wave triggering was presented. The film flow and its wave formation were decisively determined by the angle of inclination of the channel and the Reynolds number. The data were recorded at several measurement positions in order to obtain a dependency on the run length. By triggering with the confocal chromatic sensor, it is possible to selectively capture the velocity profile depending on the film thickness. The instantaneous velocity profiles were not recorded, but the data for each plane were averaged from several selected waves. Here, the focus was on the wave crest, since this can be selected very well, so that they differ only minimally. Of course, the method can also be applied to other positions in the film flow. In naturally evolving flows, unequal non-periodic waves occur, which can lead to larger scattering of velocities for positions between the wave crest and wave trough. This can be minimized by exciting the flow to produce nearly periodic identical waves. The resolution of the measurement method depends on the depth of field of the camera lens combination and the smallest possible travel distance of the camera on the linear unit. With a suitable design of the components, higher resolutions are possible through scanning than lateral viewing, but this also results in a high time expenditure, depending on how many waves are to be observed. With the measurement methodology, the averaged velocity profiles were examined as a function

of the angle of inclination, the Reynolds number and the measurement position. The results of the confocal chromatic sensor show a distinctive dependency of the wave formation on the tilt angle of the channel, the Reynolds number and the run length, even for small angles. The data of the individual measuring positions (300–500 mm) at the different angles show a clear velocity shift or development. Thus, despite small angles, the average velocity increases by 5–13%, while the wave amplitude increases in part by up to 250%.

In comparison to the theoretical values according to Nusselt, it was shown that with increasing waviness, the deviation from the theoretical data also increases significantly. The higher the angle of inclination, the earlier and more developed the waves are at the various measurement positions. As a result, the deviation from Nusselt increases with increasing inclination angle and distance to the inlet. Comparative measurements could show that measurements within wavy film flows are possible without triggering, but show lower velocities than with wave triggering on the wave crest. It was also shown that the flow profiles start to diverge from each other near the wave layer. This is an indication that the wave layer influences the base layer. In future, further measurements will investigate the influence of the wave layer on the base film in more detail. In addition, the parameter range should be extended in order to obtain an empirical correlation of the parameters of naturally noisy film flows depending on the material properties, Reynolds number, inclination angle and the measurement position. With a newly developed measurement methodology (Bilsing et al. 2022), velocity profiles are to be carried out and validated as 3D measurements through the temporally varying phase interface for the first time.

Author contributions Conceptualization: AM; Methodology: AM; Formal analysis and investigation: AM; Writing—original draft preparation: AM; Writing—review and editing: AM and SB; Funding acquisition: SB and UJ; Resources: UJ; Supervision: SB and UJ.

Funding Open Access funding enabled and organized by Projekt DEAL. The study was sponsored by the Industrielle Gemeinschaftsforschung (IGF) under the project number 21190 BG.

Availability of data and materials Figures have been uploaded. The related data is available and can be requested.

Declarations

Conflicts of interest The authors have no conflicts of interest to declare that are relevant to the content of this article.

Open Access This article is licensed under a Creative Commons Attribution 4.0 International License, which permits use, sharing, adaptation, distribution and reproduction in any medium or format, as long as you give appropriate credit to the original author(s) and the source, provide a link to the Creative Commons licence, and indicate if changes were made. The images or other third party material in this article are

included in the article's Creative Commons licence, unless indicated otherwise in a credit line to the material. If material is not included in the article's Creative Commons licence and your intended use is not permitted by statutory regulation or exceeds the permitted use, you will need to obtain permission directly from the copyright holder. To view a copy of this licence, visit <http://creativecommons.org/licenses/by/4.0/>.

References

- Adomeit P, Renz U (2000) Hydrodynamics of three-dimensional waves in laminar falling films. *Int J Multiph Flow* 26(7):1183–1208
- Alekseenko SV, Nakoryakov VY, Pokusaev BG (1985) Wave formation on a vertical falling liquid film. *AIChE J* 31(9):1446–1460
- Al-Sibai F (2004) Experimentelle Untersuchung der Strömungscharakteristik und des Wärmeübergangs bei welligen Rieselfilmen. PhD thesis, Rheinisch-Westfälische Technische Hochschule Aachen, Aachen
- Ausner I (2006) Experimentelle Untersuchungen mehrphasiger Filmströmungen. PhD thesis, Technische Universität Berlin, Berlin
- Bilsing C, Radner H, Burgmann S, Czarske J, Büttner L (2022) 3D imaging with double-helix point spread function and dynamic aberration correction using a deformable mirror. *Opt Lasers Eng* 154:107044
- Brauner N, Maron DM (1982) Characteristics of inclined thin films, waviness and the associated mass transfer. *Int J Heat Mass Transf* 25(1):99–110
- Brauner N, Maron DM (1983) Modeling of wavy flow in inclined thin films. *Chem Eng Sci* 38(5):775–788
- Charogiannis A, An JS, Markides CN (2015) A simultaneous planar laser-induced fluorescence, particle image velocimetry and particle tracking velocimetry technique for the investigation of thin liquid-film flows. *Exp Therm Fluid Sci* 68:516–536
- Dietze GF, Al-Sibai F, Kneer R (2009) Experimental study of flow separation in laminar falling liquid films. *J Fluid Mech* 637:73–104
- Helbig K (2007) Messung zur Hydrodynamik und zum Wärmetransport bei der Filmverdampfung. PhD thesis, Technischen Universität Darmstadt, Darmstadt
- Ishigai S, Nakanisi S, Koizumi T, Oyabu Z (1972) Hydrodynamics and heat transfer of vertical falling liquid films: part 1, classification of flow regimes. *Bull JSME* 15(83):594–602
- Kohrt M (2012) Experimentelle Untersuchung von Stofftransport und Fluidodynamik bei Rieselfilmströmungen auf mikrostrukturierten Oberflächen. PhD thesis, Technische Universität Berlin, Berlin
- Lel VV, Al-Sibai F, Leefken A, Renz U (2005) Local thickness and wave velocity measurement of wavy films with a chromatic confocal imaging method and a fluorescence intensity technique. *Exp Fluids* 39(5):856–864
- Lel VV, Leefken A, Al-Sibai F, Renz U (Eds.) (2004) Extension of the chromatic confocal imaging method for local thickness measurements of wavy films. RWTH Aachen, ICMF, Yokohama, Japan
- Miyara A (1999) Numerical analysis on flow dynamics and heat transfer of falling liquid films with interfacial waves. *Heat Mass Transf* 35(4):298–306
- Mudawar I, Houpt RA (1993) Measurement of mass and momentum transport in wavy-laminar falling liquid films. *Int J Heat Mass Transf* 36(17):4151–4162
- Nusselt W (1916) Die Oberflächenkondensation des Wasserdampfes. In: *VDI-Zeitschrift*
- Olsen MG, Adrian RJ (2000) Out-of-focus effects on particle image visibility and correlation in microscopic particle image velocimetry. *Exp Fluids* 29(7):S166–S174
- Paschke S (2011) Experimentelle Analyse ein- und zweiphasiger Filmströmungen auf glatten und strukturierten Oberflächen. PhD thesis, Technische Universität Berlin, Berlin
- Takahama H, Kato S (1980) Longitudinal flow characteristics of vertically falling liquid films without concurrent gas flow. *Int J Multiph Flow* 6(3):203–215
- Takamasa T, Kobayashi K (2000) Measuring interfacial waves on film flowing down tube inner wall using laser focus displacement meter. *Int J Multiph Flow* 26(9):1493–1507
- [VDI/-Buch]. VDI-Wärmeatlas (2013) Mit 320 Tabellen (11., bearb. und erw. Aufl.). Springer Vieweg, Berlin

Publisher's Note Springer Nature remains neutral with regard to jurisdictional claims in published maps and institutional affiliations.